An analytical model of the effects of catchment elevation on the flood frequency distribution

P. Allamano,[1] P. Claps,[1] and F. Laio[1]

[1]   The effect of temperature on the flood frequency distribution in mountainous basins is examined through a minimalist analytical model. The conceptual hypothesis on which the model is grounded is the existence of a subtractive mechanism that reduces the basin-contributing area in flood formation to the fraction of basin laying below the freezing elevation at the time of occurrence of each precipitation event. This fraction depends on the watershed hypsometric curve and on the seasonal evolution of temperatures. Under this hypothesis, the probability distribution of the annual maximum discharge is analytically derived, based on simple assumptions on the stochastic process of precipitation. The shape and the moments of this distribution explicitly relate to basin hypsometry and to the seasonality of temperatures. Qualitative results show that the simple causative mechanisms can explain the attenuation of flood quantiles in high-elevation basins. Model application to 57 watersheds in the Northwestern Italian Alps effectively demonstrates the role of the hypsography in explaining the spatial variability of the mean of the flood distribution.

1.   Introduction

[2]   The study of the flood formation processes in mountainous basins has traditionally received less attention than in temperate regions. The reason is probably related to a distinct perception of a limited flood risk in the cold environments because of the mitigating effect exerted by the snowfall that does not contribute immediately to runoff. Although this perception is easy to prove using hydrologic modeling, few attempts have been made [see e.g., *Loukas*, 2002] of traducing the principle of partially contributing mountain basin into a flood frequency model. Besides the relevance of this principle for a better understanding of the flood processes, the topic assumes practical importance when affording a regional flood frequency analysis in a mountainous region. In high-elevation basins, in fact, the difficulty of gathering observations of precipitation and runoff makes it possibly more urgent than for the temperate basins the need of connecting flood frequency distributions to physically-consistent flood producing mechanisms.

[3]   The ensemble of flood-producing mechanisms, including rainfall, snowmelt, and rain-on-snow in spring, rain on frozen ground in winter, and thundershowers in summer [*Loukas et al.*, 2000; *Bacchi and Ranzi*, 2003; *Merz and Blöschl*, 2003; *Singh et al.*, 2005] might suggest the use of detailed hydrological models to produce the flood frequency curve, for example, by means of Monte-Carlo simulations [e.g., *Littlewood*, 2002; *Rahman et al.*, 2002; *Loukas*, 2002]. Such an approach however always requires some

kind of calibration of the hydrological model parameters (assisted by consistent data availability) that prevents the use of these methods for flood risk assessment in ungauged basins.

[4]   An alternative statistically sound approach considers that the different flood formation mechanisms coexisting in mountainous basins would produce flood frequency curves representable by mixed distributions [e.g., *Waylen and Woo*, 1982; *Rossi et al.*, 1984; *Buishand and Demaré*, 1990; *Alila and Mtiraoui*, 2002; *Sivapalan et al.*, 2005]. This purely statistical approach still does not prove to be effective in regional analysis, because the flood frequency distribution becomes heavily parameterized and, so far, the parameters have not been connected to physical basin characteristics.

[5]   A more promising avenue of research, at least for the understanding of the dominant processes in the flood formation, is one which introduces some physical knowledge in the construction of the flood frequency curve, usually called the derived distribution approach [see e.g., *Eagleson*, 1972; *Gottschalk and Weingartner*, 1998; *Iacobellis and Fiorentino*, 2000; *De Michele and Salvadori*, 2002]. This is the approach adopted in this work, where the flood producing mechanisms and a stochastic forcing are transposed into a flood frequency curve in parametric and analytical form. This kind of approach stems from the conviction that, in complex contexts, models with a simple and controllable framework can provide a valuable compromise between real processes and data. In this respect, the philosophy of this work is akin to that of *Eagleson* [1978], *Milly* [1994a, 1994b], *Rodriguez Iturbe et al.* [2001], *Woods* [2003], *Perona et al.* [2007] among others.

[6]   Simplifying, yet realistic, assumptions are made to keep the analytical tractability of the proposed model (sections 2 and 3). As in the cited examples, the devised

[1]Dipartimento di Idraulica, Trasporti ed Infrastrutture Civili, Politecnico di Torino, Torino, Italy.

theoretical mechanistic model find its justification in the formulation of an analytical representation of the interaction of the forcing processes with the system characteristics, allowing one to easily perform a full sensitivity analysis of model results (section 4). To answer the question if the model structure is too simple to represent the actual outcome of the complex combination of causative processes, we rely on the possibility of validating the probabilistic model. In this case, in fact, we consider also real data to validate the overall behavior of the model and verify the model representativeness on a large geographical scale. This is done by comparing the observed variability of the mean annual flood with the behavior resulting from the model application (section 5). A discussion on the results and on the open problems to be addressed in future research closes the paper.

2. Model Structure

[7] The basic conceptual hypothesis on which the model is grounded consists in the existence of an elevation-driven subtractive mechanism that reduces the active portion of the watershed in flood formation. This mechanism is identified with the concept of contributing area (A_c), defined as the portion of the basin area (A) that is immediately involved in runoff formation. Runoff forming areas have previously been associated mainly with soil water processes (for example, infiltration-excess runoff, saturation-excess runoff, subsurface streamflow) [*Eagleson*, 1972; *Wood and Hebson*, 1986; *Blöschl and Sivapalan*, 1997; *Ambroise*, 2004]. Here we take a broader view and consider runoff-forming areas to be those areas where rain falls as liquid rather than solid water. In mountainous basins, in fact, for a given flood event, the contributing area A_c depends on the elevation at which transition from solid to liquid precipitation takes place, hereafter identified, for simplicity, as the zero-degrees isothermal, $ZT(t)$, or freezing elevation. According to this definition each precipitation event produces rainfall over the fraction A_c/A of the basin below the freezing elevation and snowfall in the upper part of the basin, the latter not contributing directly to discharge.

[8] This study aims at quantifying the role of this partitioning on flood discharge, by considering the direct runoff (q) as the result of a mechanism that can be formulated as follows:

$$q = C \cdot f_c(t) \cdot h + SM(t) \qquad (1)$$

where C is the peak runoff coefficient, $f_c(t) = A_c/A$ is the contributing area fraction, with $0 \le f_c(t) \le 1$, h is the rainfall depth and t is the Julian date. We model rainfall according to the very common Poisson representation of storm arrivals in time with rate λ, each storm having a depth h modeled as an exponentially distributed random variable with mean α. A deterministic component $SM(t)$ is added to this rainfall-runoff component to account for the snow melting contribution during the warm season. Possible presence of seasonal variation in the rate λ and average rainfall intensity α could be accounted for by using a non-homogeneous marked Poisson process for rainfall.

[9] Two different interpretations of equation (1) are possible: h can be supposed to represent the total precipi-

tation volume in a given storm, in which case α and h are expressed in mm and q represents the runoff volume per unit area, again expressed in mm. Alternatively, one can suppose to determine, for each storm event, the maximum precipitation intensity averaged over a duration d, and call this intensity h. For example, the duration d can be taken equal to 1 day, in which case q is a daily discharge per unit area, with the same units as α (for example, mm/d). The duration can also be supposed to vary from basin to basin and to be equal to some critical precipitation duration, for instance the one that maximizes the instantaneous peak discharge. When h is a precipitation intensity averaged over a critical duration, equation (1) becomes analogous to the standard rational formula, and q has the form of an instantaneous discharge per unit area, again with the same units as α (for example, mm/h or mm/d). Either of these interpretations can be adopted without affecting the general results of the model: in fact, the partitioning into liquid and solid precipitation is reasonably independent of the specific duration considered. In the following we will therefore refer to q as a generic discharge value, except than in the final application where we will use instantaneous discharge data to test the model.

[10] Under these premises, the distribution of the discharge q conditioned on the Julian date t, $P_{Q|T}(q|t)$, can be found as a derived distribution. Starting from the cumulative distribution of the precipitation events, $P_H(h) = 1 - \exp(-h/\alpha)$, and using equation (1) one finds

$$P_{Q|T}(q|t) = 1 - \exp\left(-\frac{q - SM(t)}{C\alpha \cdot f_c(t)}\right), \qquad (2)$$

in which $SM(t)$ plays the role of the position parameter, and the product $C\alpha f_c(t)$ that of the scale parameter.

[11] According to the Bayes theorem, the marginal cumulative distribution of discharge $P_Q(q)$ can then be expressed as

$$P_Q(q) = \int_t P_{Q|T}(q|t) \cdot p_T(t) \cdot dt \qquad (3)$$

where $P_{Q|T}(q|t)$ is the conditional probability in equation (2) and $p_T(t)$ is the probability density function of the date of occurrence of the events. Supposing that the precipitation events form an homogeneous Poisson sequence in time, one has $p_T(t) = 1/365$, i.e. the days of occurrence have a uniform probability density function [e.g., *Ross*, 1996, p. 66].

[12] Another consequence of the Poisson hypothesis is that the probability distribution of the discharge annual extremes $P_{Q_{AM}}(q)$ assumes the form [e.g., *Coles*, 2001, p. 131]

$$P_{Q_{AM}}(q) = \exp\left(-\lambda \cdot \left(1 - P_Q(q)\right)\right) \qquad (4)$$

where Q_{AM} are the annual maxima of discharge and $P_Q(q)$ is the marginal cumulative distribution of discharge in equation (3). For a basin having very low elevations, where the contributing area fraction is constant and equal to 1 all over the year (i.e. the whole basin contributes to runoff) and the snowmelt contribution is null, the expression
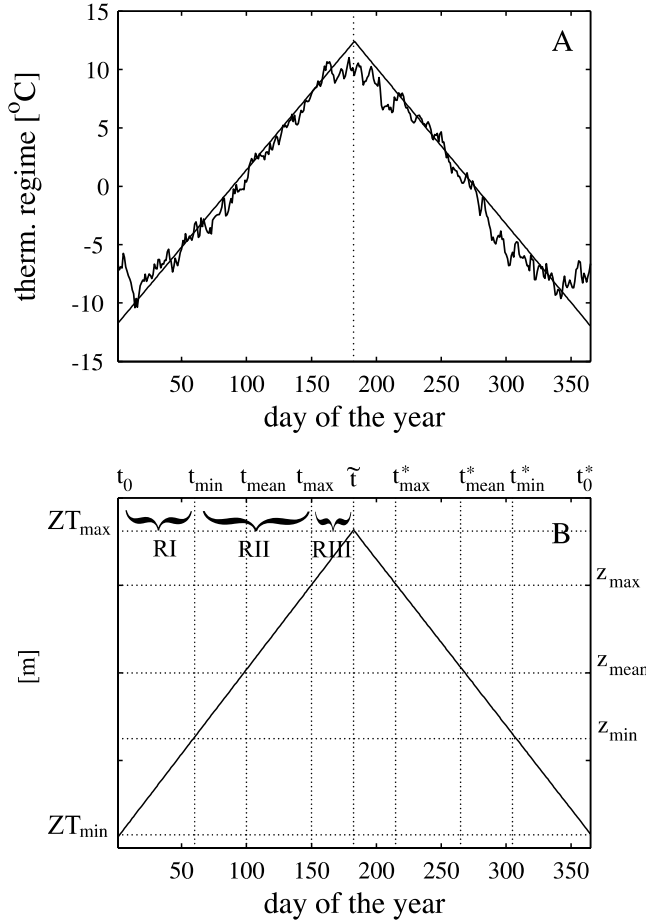
Figure 1. Panel A: example of temperature regime for the Lago Gabiet station (2340 m a.s.l.). The year starts on February, 1st. Panel B: freezing level regime obtained from the temperature regime using a constant temperature lapse rate. In the figure z_{max} and z_{min} are the maximum and minimum basin elevation, z_{mean} is the basin average elevation. ZT_{max} and ZT_{min} are the maximum and minimum values of the freezing level. t_{min}, t_{max} and t_{mean} are the instants where the $ZT(t)$ elevation equals z_{min}, z_{max}, and z_{mean}, respectively. The temporal extension of regimes RI, RII, and RIII is indicated by braces.

equation (4) reduces to the well-known form of the Gumbel distribution

$$P_{Q_{AM}}(q) = \exp\left(-\lambda \cdot \exp\left(-\frac{q}{C\alpha}\right)\right) \tag{5}$$

that we will sometimes refer to as "undisturbed" flood frequency distribution. The difference between the two curves equations (4) and (5) is a measure of the relevance of snow processes in shaping the flood frequency distribution in mountainous areas.

3. Model Specification

[13] To specify the analytical framework behind equation (3), the mathematical representations for $f_c(t)$ and $SM(t)$ are required. These representations should be necessarily simple to keep the derived distribution in analytical form.

[14] In general, $f_c(t)$ depends on t by means of the interaction between the temperature seasonality and basin hypsometry. Seasonal variation of temperature can be reproduced by a diagram of daily temperatures versus the Julian day. An example of this diagram for a mid-latitude alpine region is given in Figure 1a, where the time scale is referred to the period 1 February–31 January. In the model, only the overall shape of this diagram is reproduced, by means of a linear and symmetric curve, that we call "temperature regime". From this regime, using a constant lapse rate of temperature, one can derive the seasonal evolution of the freezing level $ZT(t)$. The interaction of this regime with the basin elevation range is represented in Figure 1b, where the rising limb of the curve follows the equation:

$$ZT(t) = \frac{ZT_{max} - ZT_{min}}{365/2} \cdot t + ZT_{min} \tag{6}$$

where ZT_{max} and ZT_{min} are the upper and lower extreme elevations occupied by the freezing level. Reference points are defined on the t-axis. The initial point $t_0 = 0$, in which $ZT(t_0) = ZT_{min}$, is assumed on 1 February. The reference day t_{min} is taken after the condition $ZT(t_{min}) = z_{min}$, with $z_{min} =$ minimum basin elevation. Accordingly, t_{mean} and t_{max} are taken after the conditions $ZT(t_{mean}) = z_{mean}$ and $ZT(t_{max}) = z_{max}$, where z_{mean} and z_{max} are the mean and maximum basin elevation, respectively. The symmetric time instants at which these conditions occur in the decreasing limb of the $ZT(t)$ migration curve are represented in the figure as t^*_{max}, t^*_{mean} and t^*_{min}. Thanks to this symmetry, from here onward equations are expressed over a six-months period lasting from t_0 to $\tilde{t}$, with $\tilde{t} = 365/2$ falling on 1 August, and then extended to the whole year. On the basis of these reference times we define as regime RI, the time interval between t_0 and t_{min}, as regime RII the interval between t_{min} and t_{max} and as regime RIII the one between t_{max} and $\tilde{t}$. Intuitively, regime RI coincides with the winter season, in which snow accumulates; regime RII coincides with spring or fall seasons and regime RIII with summer.

[15] To obtain the analytical form of the curve describing the seasonality of the contributing area fraction $f_c(t)$, the seasonal regime of the freezing level $ZT(t)$ needs to be combined with an analytical description of the watershed hypsometry (Figure 2). More or less detailed descriptions can be adopted for the distribution of elevations of a catchment, that produce more or less complicated forms for $f_c(t)$. Leaving these details to the next section, here we focus on how the migration of the freezing level reflects into the form of $f_c(t)$ and, in general, into the model structure. In fact, some of the characteristics of the $f_c(t)$ curve, as for example the fact that $f_c(t)$ is necessarily bounded between zero (during regime RI, when there is no contributing area) and 1 (during regime RIII, when the whole basin contributes), are valid per se and do not depend on the form of the hypsographic curve. The macroscopic structure of the contributing area fraction is then

$$f_c(t) = \begin{cases} 0 & \text{if } t_0 < t < t_{min} \\ 0 \div 1 & \text{if } t_{min} < t < t_{max} \\ 1 & \text{if } t_{max} < t < \tilde{t}. \end{cases} \tag{7}$$

This form, that retains the symmetric character of the temperature regime, affects the general model structure by
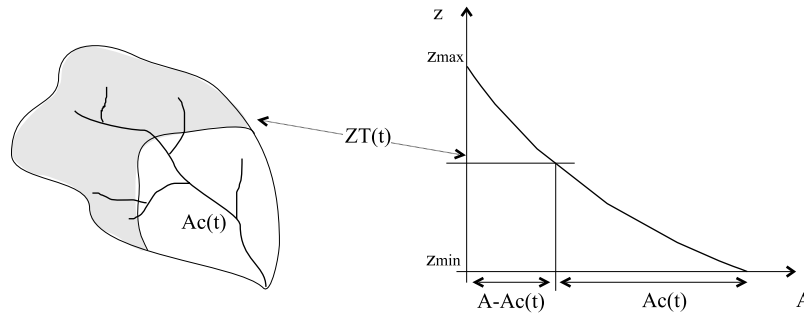
Figure 2. Schematic representation of the interaction of the freezing level elevation $ZT(t)$ with the basin elevations, represented by the hypsometric curve on the right side. The contributing fraction $A_c(t)$ of the basin is painted in white and lies below the freezing level $ZT(t)$.

inducing a redistribution of the probabilities of occurrence of the events along the year. With reference to the three aforementioned regimes, the marginal cumulative distribution of discharge $P_Q(q)$ in equation (3) can then be expressed as the combination of the corresponding probabilities pertaining to periods RI, RII and RIII

$$P_Q(q) = W_I \cdot P_I(q) + W_{II} \cdot P_{II}(q) + W_{III} \cdot P_{III}(q) \qquad (8)$$

where the weights W_I, W_{II}, and W_{III} depend on the relative durations of regimes RI, RII and RIII (see Appendix A for details). However, since $f_c(t) = 0$ between t_0 and t_{min} implies a null probability of occurrence of the events during regime RI (i.e., $P_I(q) = 0$), equation (8) becomes

$$P_Q(q) = W_{II} \cdot P_{II}(q) + W_{III} \cdot P_{III}(q), \qquad (9)$$

where W_{II} and W_{III} sum up to 1. Another consequence of $f_c(t) = 0$ during regime RI is that the average annual number of flood events in equation (4) reduces from λ to

$$\lambda^* = \lambda \cdot \frac{\tilde{t} - t_{min}}{365/2} = \lambda \cdot \frac{ZT_{max} - z_{min}}{ZT_{max} - ZT_{min}}. \qquad (10)$$

[16] Before specifying expressions for $P_{II}(q)$ and $P_{III}(q)$, the other main causative mechanism in equation (1) has to be specified. Snowmelt $SM(t)$ is again assumed to depend on the temperature regime and, as a consequence, on the Julian day t. In winter, for example, it is reasonable to consider $SM(t)$ close to zero, as $f_c(t)$, while the snowmelt tends to increase during regime RII and to reach its maximum during regime RIII. The behavior of $SM(t)$ is therefore similar to that of $f_c(t)$. For simplicity we then assume $SM(t)$ to be a linear function of $f_c(t)$ as

$$SM(t) = SM^* \cdot f_c(t) \qquad (11)$$

where the coefficient SM^* derives by an equivalence between the total volume of accumulated snow and the total melted volume:

$$\frac{R}{365} \int_0^{\tilde{t}} (1 - f_c(t)) \cdot dt = SM^* \cdot \int_0^{\tilde{t}} f_c(t) \cdot dt, \qquad (12)$$

being R the total annual rainfall amount.

[17] On the basis of the specification of the forms of $f_c(t)$ and $SM(t)$, we can now define the probability distribution pertaining to periods RII and RIII. For the regime RIII (where $f_c(t) = 1$) the expression for $P_{III}(q)$ can be derived from equation (2) as

$$P_{III}(q) = 1 - \exp\left(-\frac{q - SM^*}{C\alpha}\right) \qquad (13)$$

where the dependency on t has disappeared.

[18] The derivation of $P_{II}(q)$, which is a key point of the procedure, directly depends on the form of $f_c(t)$. Two hypotheses on the form of $f_c(t)$ have been made: a very simple description (1), called "threshold model", that considers the whole basin as hypothetically concentrated at its mean elevation z_{mean} and a more realistic description (2), called "hypsometric model", in which elevations are represented by means of an hypsometric curve.

3.1. Threshold Model (a)

[19] In the threshold model the whole basin area is considered to be concentrated at the mean basin elevation. As a consequence, $z_{min} \equiv z_{mean} \equiv z_{max}$, $t_{min} \equiv t_{mean} \equiv t_{max}$, and regime RII disappears. The seasonal curve of the contributing area fraction (equation (7)) reduces to the symmetric step function

$$f_c(t) = \begin{cases} 0 & \text{if } t < t_{mean} \\ 1 & \text{if } t > t_{mean}, \end{cases} \qquad (14)$$

where the switching times correspond to the instants when the zero degrees isothermal regime crosses the mean watershed elevation. This is exemplified in Figure 3, panels A and B, where two watersheds, having different mean elevation, are considered.

[20] The snowmelt coefficient is obtained by introducing equation (14) in equation (12), as

$$SM^* = \frac{R}{365} \cdot \left[\frac{365/2}{\int_{t_{mean}}^{365/2} f_c(t)dt} - 1 \right] = \frac{R}{365} \cdot \frac{t_{mean}}{T_s/2}, \qquad (15)$$

where $T_s = (t^*_{mean} - t_{mean})$ is the time interval when the freezing elevation overcomes the watershed mean elevation
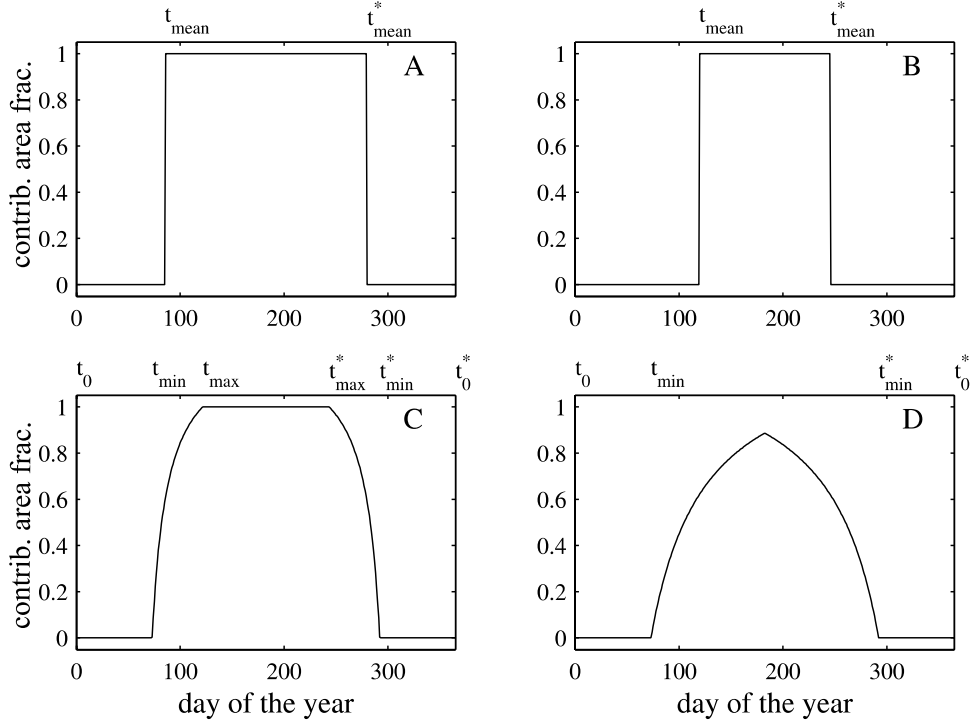
Figure 3. Contributing area fraction, $f_c(t)$, as a function of the Julian day in various configurations. All curves have the same parameter set: $\zeta = 3.3$, $ZT_{min} = 0$ m, $ZT_{max} = 3000$ m, $z_{min} = 1200$ m, except for z_{max} that is 2000 m for panels A and C and 4000 m for panels B and D. Panel A: $f_c(t)$ curve for a bounded watershed obtained with the threshold model. Panel B: $f_c(t)$ for a high-elevation watershed obtained with the threshold model. Panel C: $f_c(t)$ curve for a bounded watershed obtained using the hypsometric model. Panel D: $f_c(t)$ for a high-elevation watershed resulting from the hypsometric model.

(regime RIII) and snowmelt occurs. Equation (11) reduces to

$$SM(t) = \begin{cases} 0 & \text{if } t \in T_s \\ SM^* & \text{if } t \notin T_s \end{cases} \qquad (16)$$

where snowmelt is produced at a constant rate SM^* during T_s, while snow is considered to accumulate during the remaining period, that lasts $[365 - T_s]$ days. An increase in the mean basin elevation induces a reduction of the interval T_s and an increase in the accumulated volume, being SM^* in equation (15) inversely proportional to T_s.

[21] Given the above assumptions, $W_{III} = 1$ in equation (9) and $P_Q(q)$ assumes the form outlined in equation (13). The flood distribution is found by introducing λ^* and $P_Q(q)$ into equation (4), obtaining

$$P_{Q_{AM}}(q) = \exp\left(-\lambda^* \cdot \exp\left(-\frac{q - SM^*}{C\alpha}\right)\right). \qquad (17)$$

This curve is plotted as a solid black line in Figure 4 for two basins having different mean elevations. In the same diagram the grey thick line represents the undisturbed flood frequency distribution (equation (5)). Further comments on the shapes of these functions and an explanation for the dashed black curve are given in the following section.

3.2. Hypsometric Model (b)

[22] A more realistic representation of the distribution of elevations within a watershed is given by the hypsometric curve, which is the cumulative frequency curve of elevations of all the points in a basin. A mathematical approximation of the empirical hypsometric curve is used by adopting the one-parameter function [Strahler, 1952]:

$$\frac{z - z_{min}}{z_{max} - z_{min}} = \frac{f_c(t)}{1 + \zeta \cdot (1 - f_c(t))}, \qquad (18)$$

where z (with $z_{min} < z < z_{max}$) is the elevation that partitions the watershed into a contributing and non-contributing area and ζ is a parameter controlling the flexure of the curve, that assumes only values greater than -1. Setting the freezing elevation $ZT(t)$ for z in equation (18), one finds a piecewise expression for the contributing area fraction

$$f_c(t) = \begin{cases} 0 & t_0 < t < t_{min} \\ \dfrac{(1 + \zeta)(ZT(t) - z_{min})}{\zeta(ZT(t) - z_{min}) + z_{max} - z_{min}} & t_{min} < t < t_{max} \\ 1 & t_{max} < t < \tilde{t}. \end{cases} \qquad (19)$$

In this case the no-flood interval is $[t_0 - t_{min}]$, which produces λ^* according to equation (10).

[23] Given the above assumptions, the hypsometric model further specifies into different sub-cases, that refer to watersheds interacting with the $ZT(t)$ curve in different ways (see Table 1): a case (b1) which refers to a watershed having $z_{min} > ZT_{min}$ and $z_{max} < ZT_{max}$ (called "bounded watershed"), where all regimes RI, RII, and RIII actually exist; a case (b2) (called "high-elevation watershed") which presents
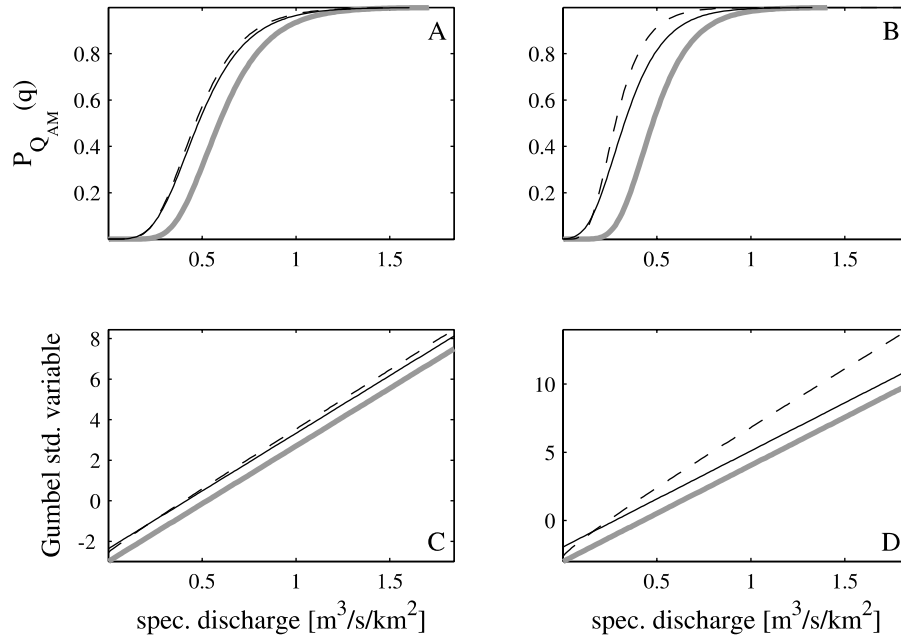
Figure 4. Cumulative probability functions $P_{Q_{AM}}(q)$ resulting from the threshold and hypsometric models (respectively, black solid and dashed lines) compared to the form of the undisturbed flood frequency distribution (grey thick line). The same probability functions are compared on a Gumbel probability plot (panels C–D). All curves are related to the same parameter set: $C = 0.5$, $\alpha = 40$ mm/d, $\lambda = 20$ [1/yr], $\zeta = 3.3$, $z_{min} = 1200$ m, except for z_{max} that is 2000 m for curves in A and C and 4000 m for curves in B and D. As a consequence, panels A and C refer to the bounded watershed typology, panels B and D to the high-elevation case.

$z_{max} > ZT_{max}$ and consequently admits regimes RI and RII only; a case (b3), having $z_{min} \leq ZT_{min}$ and $z_{max} \leq ZT_{max}$ (called "warm bounded watershed") and a case (b4), having $z_{min} \leq ZT_{min}$ and $z_{max} > ZT_{max}$ (called "warm high-elevation watershed"). Cases (b1) and (b2) are the most common at mid-latitudes, where the zero degrees isothermal can be assumed to range between $ZT_{min} = 0$ m a.s.l. in February and approximately $ZT_{max} = 3000$ m a.s.l. in August (ensuring that $z_{min} > ZT_{min}$), while the other cases refer to warmer climates where $ZT_{min} > 0$ m a.s.l in February. In Appendix A the discharge probability distributions are derived for all these cases however in the application only cases (b1) and (b2) are taken into account.

[24] The seasonal representation of $f_c(t)$ for the bounded watershed is shown in Figure 3c and the analytical form of $P_Q(q)$ is provided in equation (A5). An example of the resulting cumulative probability function $P_Q(q)$ is plotted (as a dashed line) in Figure 4a, beside the undisturbed flood frequency distribution (grey thick line) and the one obtained with the threshold simplification (solid line). The parameter values are assigned to reproduce the typical situation in a temperate basin. Both curves (dashed and solid), compared to the undisturbed one (equation (5)), show a leftward shift, that is more marked for the curve resulting from the hypsometric model. The curves are also compared on a Gumbel probability plot (Figure 4c), where one can observe that the shift between the undisturbed and threshold curve is constant while the hypsometric curve deviates moving to higher elevations. This behavior can be ascribed to the form of the snowmelt function $SM(t)$, that is constant in the threshold model and time-dependent in the hypsometric model (see Appendix A1 for details).

[25] For a high-elevation watershed the $f_c(t)$ curve is represented in Figure 3d. The procedure for the derivation of the $P_Q(q)$ remains almost the same, except for the absence of regime RIII. The corresponding $P_{Q_{AM}}(q)$ is plotted (as a dashed line) in Figure 4b, compared to the undisturbed curve (grey thick line) and to the one obtained with the threshold simplification (solid line). Analogously to the previous case, the curves are also compared on a

Table 1. Overview of the Cases Taken Into Account in This Study[a]

	Bounded $z_{min} > ZT_{min}$; $z_{max} < ZT_{max}$	High-Elevation $z_{min} > ZT_{min}$; $z_{max} > ZT_{max}$	Warm-Bounded $z_{min} \leq ZT_{min}$; $z_{max} < ZT_{max}$	Warm-High $z_{min} \leq ZT_{min}$; $z_{max} > ZT_{max}$
Threshold model	(a1) RI, RIII	(a2) RI, RIII	(a3) RIII	(a4) RIII
Hypsometric model	(b1) RI, RII, RIII	(b2) RI, RII	(b3) RII, RIII	(b4) RII

[a]Columns contain the basin typologies, rows the simplified (threshold) and hypsometric model formulations. Columns-rows crossings contain the regimes that actually occur under each formulation, being $f_c(t) = 0$ during regime RI, $f_c(t) = 1$ during regime RIII and $0 < f_c(t) < 1$ during regime RII.
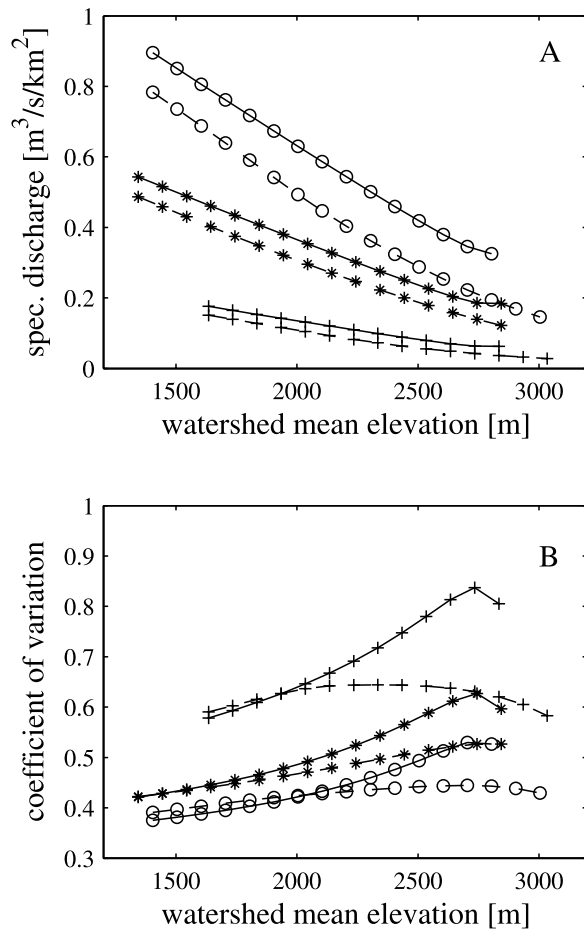
Figure 5. Panel A: modeled values of mean specific peak discharge versus basins average elevation. Panel B: *CV* from the model versus basins mean elevation. Solid curves refer to the threshold model; dashed curves to the hypsometric model. Stars, circles, and plus signs refer to different parameterizations. In particular, ZT_{min} and ZT_{max} are kept constant and equal to 0 and 3000 m a.s.l. respectively, and the basin elevation range is set to 2000 m starting at the same z_{min}. Stars refer to the parameter set: $C = 0.5$, $\alpha = 40$ mm/d, $\lambda = 20$ [1/yr], $\zeta = 3.3$, circles to: $C = 0.5$, $\alpha = 60$ mm/d, $\lambda = 30$ [1/yr], $\zeta = 0.33$ and plus signs to: $C = 0.5$, $\alpha = 20$ mm/d, $\lambda = 10$ [1/yr], $\zeta = -0.33$.

Gumbel probability plot (Figure 4d) where a more marked shift than in the bounded watershed case is observed.

4. Model Sensitivity

[26] In this section the attitude of the model to represent realistically flood processes in mountainous basins is explored using "synthetic" case-studies, identified by different parameter sets that trace back to the cases of bounded and high-elevation watersheds (see Table 1 for an overview of all the possible cases). In general the following classes of parameters have to be specified:

[27] (1) Geometric parameters, describing watershed hypsometry, such as the maximum (z_{max}) and minimum (z_{min}) elevations of the watershed and the parameter ζ controlling the shape of the hypsometric curve. ζ results

from the equivalence between the integral of the hypsometric curve and the normalized mean watershed elevation.

[28] (2) Climatic parameters at the basin scale, i.e. α and λ for the rainfall model and the total annual rainfall R. To keep the analytical tractability of the model we assume α and λ to be constant all over the year. The introduction of a seasonal regime of α and λ, in fact, would be more realistic but would make the model much more complicated. We also assume R to be proportional to α through a parameter k, so that α becomes the scale parameter of the model.

[29] (3) Climatic parameters related to the macro-region, such as the maximum (ZT_{max}) and minimum (ZT_{min}) values of the freezing level migration curve. Observe that by setting the two limits on the $ZT(t)$ one assumes that the temperature regime of the region has already been transposed into the freezing level curve. This is done using a constant temperature lapse rate (that usually ranges between $5° \div 7°$C every 1000 m of elevation).

[30] In our analysis, the degrees of freedom of the parameters space are further reduced by setting the temperature lapse rate to 7°C/1000 m, with a consequent range of the freezing level going from $ZT_{min} = 0$ m a.s.l. to $ZT_{max} = 3000$ m a.s.l. during the year. It is also assumed that the parameter k is constant, defining the total annual rainfall as $R = 30 \times \alpha$.

[31] In Figures 5a and 5b the mean values of the simulated specific peak discharges as well as their coefficients of variation are related to the mean watershed elevation. Stars, circles and plus signs allow one to discern among three different parameter sets. Solid lines refer to the threshold model, dashed lines to the hypsometric model. The negative slope of the curves in panel A is due to the effect of the reduction of the contributing area with elevation, formally expressed by equation (1). For two out of three parameterizations the range of values covered by the solid curves is shorter than the one covered by the dashed curves. This is because of the implicit assumption in the threshold model of the mean elevation being necessarily lower than ZT_{max}. As a consequence, the final points of the curves, that represent basins located at higher elevations, in some cases cannot be modeled under the hypotheses of the threshold model.

[32] The model also produces an increase of the coefficient of variation moving from low- to mid-elevation basins and then a reduction of CV for high-elevation watersheds. The final drop is due to the snowmelt component of the model that reduces the variance and raises the mean of the discharge values.

5. Model Application

[33] In this section the model is tested using data from 57 watersheds located in the North-Western Italian Alps (over an area of almost 30000 km², see Figure 6). The basins are selected according to the availability of records of maximum annual peak discharge. The watersheds considered present mean elevations ranging from 470 to 3100 m a.s.l. and very different sizes, as areas vary between 22 and 7650 square kilometers (for additional information see auxiliary materials at http://www.idrologia.polito.it/~allamano/lavori/dataset.txt). The wide spectrum of basin characteristics will help to demonstrate the robustness of the model results, concerning the spatial variability of the mean.
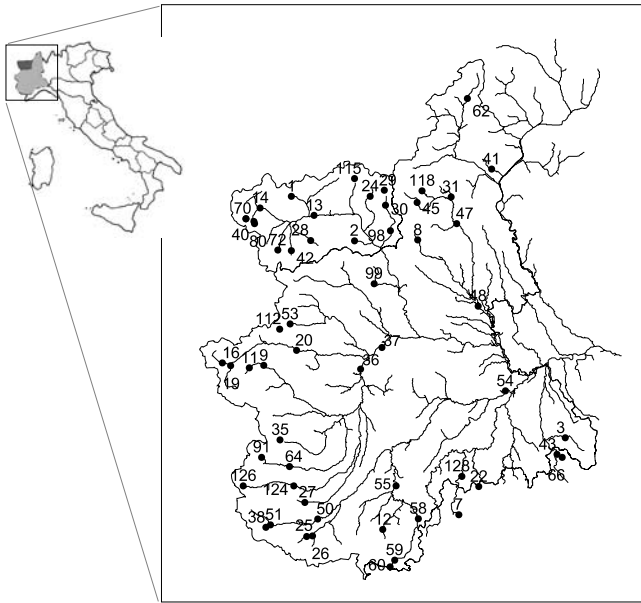
Figure 6. Geographic position of the basins outlets. The map in the top left corner indicates the location of the region of study in Italy.

[34] Since we are interested in investigating the relations between the characteristics of the flood distribution and basin elevation, we first look at how the first two moments of the series of annual maxima vary with the average basin elevation. Figure 7a shows the dependence of the specific (i.e. per unit area) mean peak discharge on average basin elevation for the 57 basins. A significant decreasing trend is found (with p value = 2.65×10^{-6}) that could reasonably be ascribed to the contributing area effect, in agreement with the behavior suggested in Figure 5a. In Figure 7b, the coefficients of variation of the annual maxima are plotted versus basin elevation. The dependence on elevation is here more noisy and not monotonic, so that neither the behavior suggested in Figure 5b nor other dependencies on elevation can be recognized.

[35] On these bases one could argue that also the variation with elevation of other descriptors, like basin area or average precipitation, could possibly induce significant deviations in the relations between the moments of flood frequency curves and elevation. For example, among gauged basins, those with higher average elevation are typically smaller than the lower ones (Figure 8a). In addition, the 1-hour maximum precipitation changes when moving to higher-elevation regions [e.g., *Kuzuha et al.*, 2006]. This effect is represented in Figure 8b, where the rainstorm index h_1, obtained by spatially interpolating the mean of the measured annual maximum precipitation in 1 hour and then averaging them on the basin area, is related to the mean watershed elevation. A significant decreasing trend is observed (p value = 4.5×10^{-16}), that we found also when broadening the analysis to the whole Italian territory (2555 rain gauging stations). This latter decreasing trend can be taken as an indication for the behavior of generic short-duration annual maximum precipitation.

[36] The relation between mean specific discharge and average elevation in Figure 7a could then be the result of the

variations of these factors with elevation. Our data however demonstrate that this is not the case. In fact the specific discharge generally increases with decreasing catchment areas, which would imply (from Figure 8a) an increase of the specific discharge with the average basin elevation. A coherent decreasing trend with elevation is instead shown by precipitation. In fact the average of the annual maximum precipitation in 1 hour (h_1) decreases with mean basin elevation (Figure 8b). However the slope of the trend is much lower than the slope of the regression line found from the mean discharge data in Figure 7a. This implies that precipitation may be a concurring factor but its relation with elevation is not sufficient to explain completely the decreasing trend of Figure 7a. On these bases, the dependence of precipitation on elevation is also taken into account into the model, by relating the average of the hourly annual maximum precipitation h_1 to the α parameter. α is scaled to α^* according to the relation $\alpha^* = \alpha \left(1 - (z_{mean}/D)\right)$, in which an estimate for parameter D (= 3800 m) is obtained with the linear regression shown in Figure 8b.

[37] So far the ability of the model to explain the relation between mean floods and elevation has not been quantita-
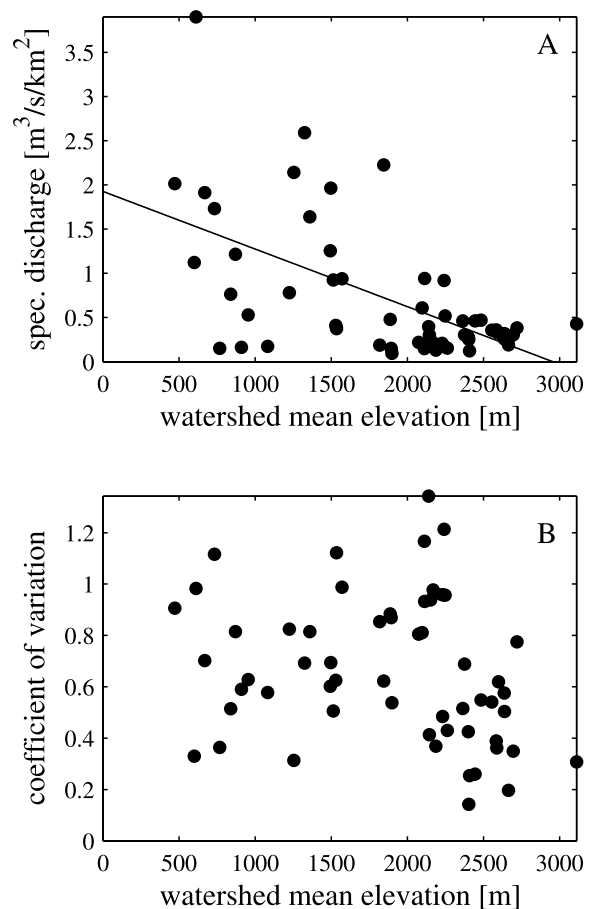

Figure 7. Panel A: relationship between mean specific (i.e., divided by catchment area) peak discharge and watershed average elevation for the 57 basins considered in the North-Western Italian Alps. Solid line represents the fitted regression line (p value = $2.65 \cdot 10^{-6}$). Panel B: empirical values of CV for the same series versus basin average elevation.
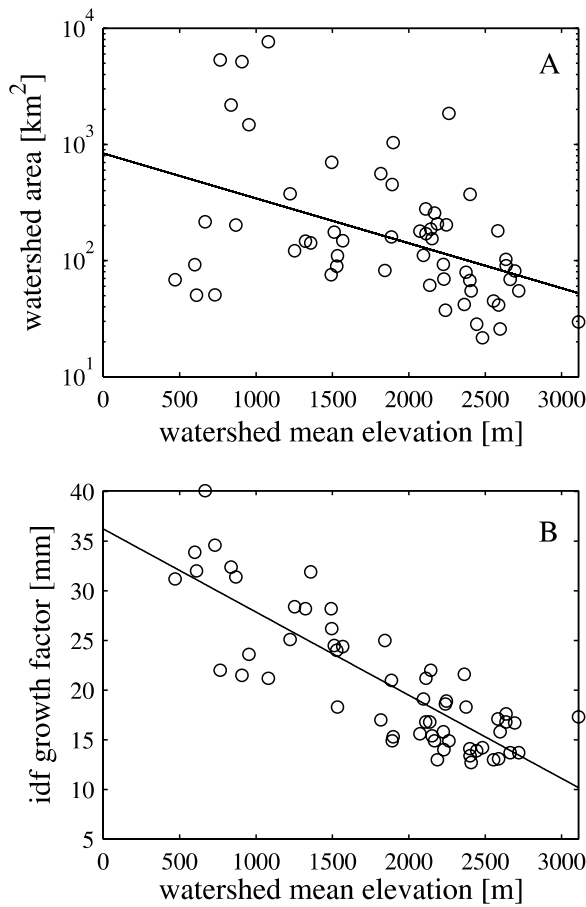
Figure 8. Panel A: basin area plotted versus basin average elevation (note the log y-axis). Circles refer to the database of watersheds from the North-Western Italian Alps. Solid lines represent the fitted linear regression lines (p value = 0.004). Panel B: growth factor h_1 of the intensity-duration-frequency curve ($h = h_1 \cdot d^n$, where d is the duration in hours) versus watershed mean elevation (p value = 4.5×10^{-16}).

tively demonstrated. Now we move to a quantitative verification of the model. To test if the empirical evidence observed in Figure 7 is likely to be explained by the mechanism suggested in equation (1) we use the model to evaluate, for each basin, how would the mean specific discharge change if the basin was moved to the sea level, where of course no elevation effect is present. To this aim, we estimate the two climatic parameters $C\alpha$ and λ for a set of real basins. We refer to $C\alpha$ instead of α, because we base our estimation on discharge rather than on precipitation data. Therefore we have to take into account the reduction of effective precipitation compared to precipitation according to the concept of "peak runoff coefficient".

[38] In the proposed model the first and second moment of the distribution of the discharge extremes are functions of $C\alpha$ and λ

$$\mu_{mod} = \int_0^\infty p_{QAM}(q) \cdot q \cdot dq = \Psi_1(C\alpha, \lambda)$$

$$\sigma_{mod} = \int_0^\infty p_{QAM}(q) \cdot (q - \mu_{mod})^2 \cdot dq = \Psi_2(C\alpha, \lambda) \quad (20)$$

where $\Psi_1(C\alpha, \lambda)$ and $\Psi_2(C\alpha, \lambda)$ depend on the cases presented in the appendix and are not necessarily expressed in closed form.

[39] In contrast the coefficient of variation $CV_{mod} = \sigma_{mod}/\mu_{mod}$ is only a function of λ, because $C\alpha$ is a scale parameter for the distribution $P_{QAM}(q)$. By equating the expressions of CV_{mod} and μ_{mod} to their empirical counterparts one obtains the estimators of $C\alpha$ and λ which, of course, differ from basin to basin. We can now use these estimated values of $C\alpha$ and λ into equation (5), to obtain the corresponding mean and CV

$$\mu = C\alpha \cdot (\ln \lambda + \gamma_E)$$

$$CV = \frac{\pi}{\sqrt{6}(\ln \lambda + \gamma_E)} \quad (21)$$

where γ_E is the Euler constant. The values of μ and CV in equations (21) can be interpreted as the mean and coefficient of variation for a basin which is identical to the one under consideration, but in which no elevation effects are experienced.

[40] In Figure 9a, these estimated moments are compared to their empirical counterparts, corresponding to the points in Figure 7a. For each basin a couple of points is plotted: the black circle represents the observed mean specific discharge while the grey circle is the corresponding value that would be measured if the effects induced by the basin elevation were removed (equation (21)). Greater displacements between the two points correspond to higher-elevation watersheds, where the elevation effect is more relevant. Grey points represent in fact flood statistics for fictitious basins having the same (null) average elevation, with identical parameters of the precipitation forcing estimated on the series of the real basins. This in turn implies that for the grey points the watershed mean elevation should not appear as an explanatory variable for μ if the model works correctly. It can be recognized that no trend is detectable for the regression line of the grey points in Figure 9. This demonstrates the model ability to explain (and then to remove) the relation between mean peak floods and elevation in the absence of any calibration.

[41] Considering the CV, instead, the displacements of the grey points obtained looks non systematic. Moreover some residual dependence (not statistically significant) of the CV on elevation results after the displacement (Figure 9b). Experimental points of CV (Figure 7b) are in fact very scattered, and also the curves suggested in Figure 5b do not show a clear dependence of CV on elevation. This confirms that, if any, the relation between the CV and basin hypsography is still to be understood, even at the empirical level.

6. Discussion and Conclusions

[42] The role of the temperature regime and of the distribution of elevation in mountainous basins is investigated through a minimalist analytical model of the flood formation mechanisms. A derived distribution approach is used to produce a flood frequency curve by the superimposition of the precipitation and temperature regimes, conditioned on the actual basin elevations. Qualitative results demonstrate that the simple causative mechanisms
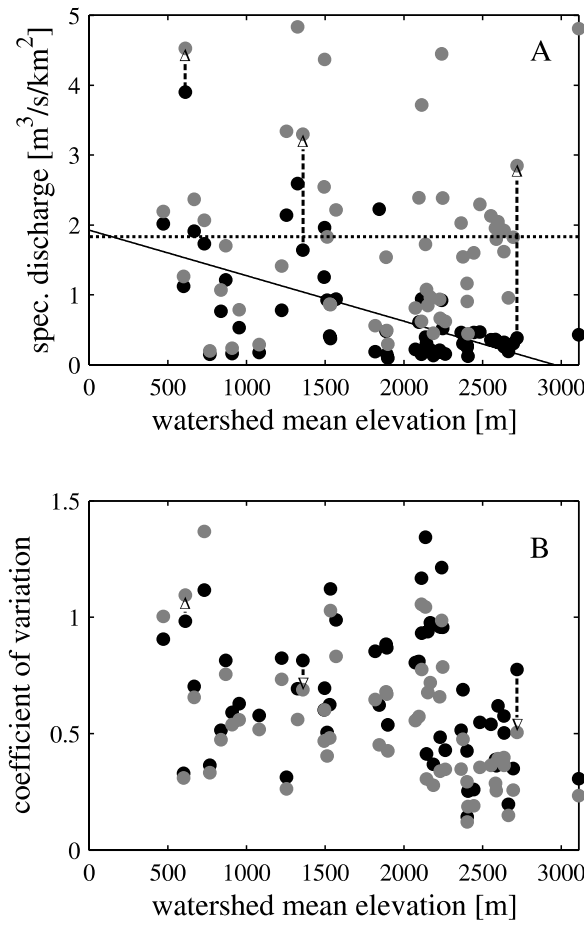
Figure 9. Panel A: mean specific peak discharge values versus watersheds mean elevation. Black circles represent empirical means, as in Figure 7a. Grey points are means recomputed by removing the elevation effect (procedure outlined in section 5). The solid curve is fitted on observed points (p value = 2.65×10^{-6}), the dotted line is fitted on the recomputed values (p value = 0.99). Dashed vertical traits demonstrate the entity of the displacement between the points. The displacement is shown to increase with average elevation Panel B: CV versus basin average elevation. Black circles represent the empirical points, as in Figure 7b. Grey points are recomputed values obtained as outlined in section 5.

incorporated in the model can explain the characteristic attenuation of flood quantiles in high-elevation basins. Quantitative results, for 57 alpine basins, confirm this finding. It is important to observe that the result is obtained with a model where all parameters are fixed a priori or estimated from the data, i.e. without any calibration that could adjust the slope of the regression line. This is, in our opinion, a very positive result which entails that the model is actually able to explain the variability induced by basin elevation on the average specific flood discharge. Residual variability is observed, possibly ascribable to the effect of other mechanisms that are not included in the actual model structure. In contrast, the modeling scheme does not help to explain the dependence,

if any, of the empirical coefficient of variation with elevation.

[43] Further increase in model complexity is always possible, that would perhaps impact the final flood distribution. For example the model in its current formulation does not take into account the rain-on-snow effect, that is known to be a significant triggering mechanism for alpine flood events that increases the non-linearity of the response. It is also of interest to evaluate the impact of non-uniform rate of precipitation within the year. Both variants will be the subject of future analyses. However it must be kept in mind that the documented strong variability and the frequent errors in precipitation measurement in high-elevation sites [*Sevruk*, 1983] will always create difficulties in the model validation. In this sense, the challenge of this research is not only to improve models but also to focus on the need of using objective measures for model verification. Moreover given the simple structure of the model it seems that the model could successfully be used for "first order" investigations of the changing nature of flood risks in mountain environments subject to warming temperatures.

Appendix A: Analytical Solutions of the Equations

[44] The procedure to obtain an analytical representation of equation (3) is described for watersheds having different elevation characteristics (see Table 1).

A1. Bounded Watershed (b1)

[45] The bounded watershed is characterized by $z_{\min} > ZT_{\min}$ and $z_{\max} < ZT_{\max}$. As a consequence, the $f_c(t)$ curve is non-null in periods RII and RIII (Figure 3c). Regime RII is weighted by a factor

$$W_{II} = \frac{t_{\max} - t_{\min}}{\tilde{t} - t_{\min}} = \frac{z_{\max} - z_{\min}}{ZT_{\max} - z_{\min}}, \quad (A1)$$

which accounts for the relative duration of regime RII and, analogously, regime RIII with

$$W_{III} = \frac{\tilde{t} - t_{\max}}{\tilde{t} - t_{\min}} = \frac{ZT_{\max} - z_{\max}}{ZT_{\max} - z_{\min}}. \quad (A2)$$

The expression for $P_{II}(q)$ to substitute in equation (9) becomes

$$
\begin{aligned}
P_{II}(q) &= 1 - \frac{\exp\left(\frac{SM^*}{C\alpha}\right)}{t_{\max} - t_{\min}} \cdot \int_{t_{\min}}^{t_{\max}} \exp\left(-\frac{q}{C\alpha f_c(t)}\right) dt \\
&= 1 - \exp\left(\frac{SM^* - q}{C\alpha}\right) \\
&+ \frac{q \cdot \exp\left(\frac{SM^* + \zeta SM^* - \zeta q}{C\alpha(1+\zeta)}\right) \cdot \Gamma\left[0, \frac{q}{C\alpha(1+\zeta)}\right]}{C\alpha \cdot (1+\zeta)}
\end{aligned}
$$
(A3)

where $f_c(t)$ is given by equation (19) and $\Gamma[a,z] = \int_0^\infty t^{a-1} e^{-t} dt$ is the incomplete gamma function [*Abramowitz and Stegun*, 1965, sec. 5].

[46] Using equation (12) the SM^* factor is obtained as

$$SM^* = \frac{R}{365} \cdot \frac{\zeta(\Delta z - \zeta B) - (1+\zeta)\Delta z \ln[1+\zeta]}{\zeta(\zeta D - \Delta z) + (1+\zeta)\Delta z \ln[1+\zeta]}, \quad (A4)$$

w h e r e $\Delta z = (z_{max} - z_{min})$, $B = (z_{min} - ZT_{min})$ a n d $D = (z_{min} - ZT_{max})$. By introducing equations (13), (A1), (A2), (A3) and (A4) in equation (9) one finds

$$P_Q(q) = 1 - \exp\left(\frac{SM^* - q}{C\alpha}\right)$$
$$- \frac{\exp\left(\frac{SM^*(1+\zeta) - \zeta q}{C\alpha(1+\zeta)}\right) \cdot q\Delta z \cdot \Gamma\left[0, \frac{q}{C\alpha(1+\zeta)}\right]}{C\alpha \cdot D(1+\zeta)}. \quad (A5)$$

To obtain the distribution of the extremes, one should replace the term $P_Q(q)$ of (A5) in equation (4), where equation (10) should be used to account for the effects of regime RI on the reduction of λ.

A2. High-Elevation Watershed (b2)

[47] For a high-elevation watershed (having $z_{min} > ZT_{min}$, $z_{max} > ZT_{max}$) the procedure for the derivation of $P_Q(q)$ remains almost the same, except for the absence of regime RIII (Figure 3d). This absence changes the integration interval in equations (12) and (A3) into $[t_{min} - \widetilde{t}]$ and allows one to obtain, by analytical integration

$$SM^* = -\frac{R}{365}\left(1 + \frac{\zeta^2 \cdot \Delta ZT/(1+\zeta)}{\zeta D - 2\Delta z \cdot \text{ATh}\left[-\frac{\zeta D}{(\zeta D - 2\Delta z)}\right]}\right), \quad (A6)$$

where D is as previously defined, $\Delta ZT = (ZT_{max} - ZT_{min})$ and $\text{ATh}[-]$ is the hyperbolic arc-tangent.
[48] The expression of $P_Q(q)$ is therefore

$$P_Q(q) = 1 - \exp\left(\frac{q(\Delta Z - \zeta D)}{(1+\zeta)D/C\alpha} + \frac{SM^*}{C\alpha}\right) - \frac{q\Delta z}{C\alpha(1+\zeta)D}$$
$$\cdot \exp\left(\frac{SM^*(1+\zeta) - q\zeta}{C\alpha(1+\zeta)}\right) \cdot \text{EI}\left[1, -\frac{q\Delta z}{C\alpha(1+\zeta)D}\right], \quad (A7)$$

where $\text{EI}[n, z] = \int_1^\infty (e^{-zt}/t^n)dt$ is the exponential integral function [*Abramowitz and Stegun*, 1965, sec. 6]. In order to obtain the distribution of the extremes, equation (A7) should be substituted into equation (4), again taking into account the reduction of λ (equation (10)).

A3. Warm Bounded Watershed (b3)

[49] In warmer climates, where in February $ZT_{min} > 0$, the warm counterpart of the bounded watershed b1 should be considered. This is the case of a watershed having $z_{min} \leq ZT_{min}$ and $z_{max} < ZT_{max}$, in which case one obtains:

$$SM^* = \frac{R}{365}\left(\frac{\zeta^2 \Delta ZT}{\zeta(G + \zeta\Delta ZT) - (1+\zeta)\Delta z \ln\left[\frac{(1+\zeta)\Delta z}{\Delta z + \zeta(z_{min} + ZT_{min})}\right]} - 1\right),$$
$$(A8)$$

where $G = (z_{max} - ZT_{min})$ and

$$P_Q(q) = \frac{\exp(-q/C\alpha)}{C\alpha(1+\zeta)\Delta ZT}\left(C\alpha(1+\zeta)\exp\left(-\frac{ZT_{min}q}{C\alpha(1+\zeta)B}\right)\right.$$
$$\cdot\left(\exp\left(\frac{ZT_{min}q}{C\alpha(1-\zeta)B} + \frac{SM^*}{C\alpha}\right)\right.$$
$$+ D\exp\left(\frac{q}{C\alpha}\left(1 + \frac{ZT_{min}}{B(1+\zeta)}\right)\right)\right)$$
$$\cdot \Delta ZT - B\exp\left(\frac{z_{max}q}{C\alpha(1+\zeta)B} + \frac{SM^*}{C\alpha}\right)\right)$$
$$- \exp\left(z\frac{q + SM^*(1+\zeta)}{C\alpha(1+\zeta)}\right)$$
$$\left.\cdot \Delta zq\left(\text{EI}[-qC\alpha(1+\zeta)] - \text{EI}\left[\frac{\Delta zq}{C\alpha(1+\zeta)B}\right]\right)\right). \quad (A9)$$

A4. Warm High-Elevation Watershed (b4)

[50] Analogously, for the warm high-elevation case (having $z_{min} \leq ZT_{min}$, $z_{max} > ZT_{max}$), one has

$$SM^* = \frac{R}{365}\left(\frac{\zeta^2\Delta ZT/(1+\zeta)}{\zeta\Delta ZT + 2\Delta z\text{ATh}\left[\frac{\zeta - \Delta ZT}{2\Delta z - \zeta(2z_{min} - \Delta ZT)}\right]} - 1\right), \quad (A10)$$

and

$$P_Q(q) = 1 - \frac{\exp\left(\frac{SM^*}{C\alpha} - \frac{q}{C\alpha(1+1/\zeta)}\right)}{C\alpha(1+\zeta)\Delta ZT}(-C\alpha(1+\zeta))$$
$$\cdot\left(-D\exp\left(\frac{\Delta zq}{C\alpha(1+\zeta)D}\right) - B\exp\left(\frac{\Delta zq}{C\alpha(1-\zeta)D}\right)\right.$$
$$\left.+ q\Delta z\left(\text{EI}\left[\frac{\Delta zq}{C\alpha(1-\zeta)D}\right] - \text{EI}\left[\frac{\Delta zq}{C\alpha(1-\zeta)D}\right]\right)\right).$$
$$(A11)$$

References

Abramowitz, M., and I. Stegun (1965), *Handbook of Mathematical Functions*, Applied Math. Ser. 55, National Bureau of Standards, Dover Publications, New York.

Alila, Y., and A. Mtiraoui (2002), Implications of heterogeneous flood-frequency distributions on traditional stream-discharge prediction techniques, *Hydrol. Processes*, 16, 1065–1084.

Ambroise, A. (2004), Variable "active" versus "contributing" areas periods: A necessary distinction, *Hydrol. Processes*, 18, 1149–1155.

Bacchi, B., and R. Ranzi (2003), Hydrological and meteorological aspects of floods in the Alps: An overview, *Hydrol. Earth Syst. Sci.*, 7(6), 785–798.

Blöschl, G., and M. Sivapalan (1997), Process controls on regional flood frequency: Coefficient of variation and basin scale, *Water Resour. Res.*, 33(12), 2967–2980.

Buishand, T., and G. Demaré (1990), Estimation of the annual maximum distribution from samples of maxima in separate seasons, *Stochastic Hydrol. Hydraul.*, 4, 89–103.

Coles, S. (2001), *An Introduction to Statistical Modeling of Extreme Values*, Springer Series in Statistics, Springer-Verlag, London, U.K.

De Michele, C., and G. Salvadori (2002), On the derived flood frequency distribution: Analytical formulation and the influence of antecedent soil

moisture condition, *J. Hydrol.*, *262*, 245–258.

Eagleson, P. (1972), Dynamics of flood frequency, *Water Resour. Res.*, *8*(4), 878–898.

Eagleson, P. (1978), Climate, soil and vegetation. 1. Introduction to water balance dynamics, *Water Resour. Res.*, *14*(5), 705–712.

Gottschalk, L., and R. Weingartner (1998), Distribution of peak flow derived from a distribution of rainfall volume and runoff coefficient, and a unit hydrograph, *J. Hydrol.*, *208*, 148–162.

Iacobellis, V., and M. Fiorentino (2000), Derived distribution of floods based on the concept of partial area coverage with a climatic appeal, *Water Resour. Res.*, *36*(2), 469–482.

Kuzuha, Y., M. Sivapalan, K. Tomosugi, T. Kishii, and Y. Komatsu (2006), Role of the spatial variability of rainfall intensity: Improvement of Eagleson's classical model to explain the relationship between the coefficient of variation of annual maximum discharge and catchment size, *Hydrol. Processes*, *20*, 1335–1346.

Littlewood, I. (Ed.) (2002), *Continuos River Flow in Simulation: Methods, Applications and Uncertainties*, Occasional Paper 13, British Hydrol. Soc., U.K.

Loukas, A. (2002), Flood frequency estimation by a derived distribution procedure, *J. Hydrol.*, *255*, 69–89.

Loukas, A., L. Vasiliades, and N. Dalezios (2000), Flood producing mechanisms identification in southern British Columbia, Canada, *J. Hydrol.*, *227*, 218–235.

Merz, R., and G. Blöschl (2003), A process typology of regional floods, *Water Resour. Res.*, *39*(12), 1340, doi:10.1029/2002WR001952.

Milly, P. (1994a), Climate, interseasonal storage of soil water, and the annual water balance, *Adv. Water Resour.*, *17*, 19–24.

Milly, P. (1994b), Climate, soil water storage and the average annual water balance, *Water Resour. Res.*, *30*(7), 2143–2156.

Perona, P., A. Porporato, and L. Ridolfi (2007), A stochastic process for the interannual snow storage and melting dynamics, *J. Geophys. Res.*, *112*, D08107, doi:10.1029/2006JD007798.

Rahman, A., P. Weinmann, T. Hoang, and E. Laurenson (2002), Monte Carlo simulation of flood frequency curves from rainfall, *J. Hydrol.*, *256*(3–4), 196–210.

Rodriguez Iturbe, I., A. Porporato, F. Laio, and L. Ridolfi (2001), Plants in water-controlled ecosystems: Active role in hydrologic processes and response to water stress I. Scope and general outline, *Adv. Water Resour.*, *24*, 695–705.

Ross, S. (1996), *Stochastic Processes*, John Wiley, New York.

Rossi, F., M. Fiorentino, and P. Versace (1984), Two-component extreme value distribution for flood frequency analysis, *Water Resour. Res.*, *20*(7), 847–856.

Sevruk, B. (1983), Correction of measured precipitation in the Alps using the water equivalent of new snow, *Nord. Hydrol.*, *14*(2), 49–58.

Singh, V., S. Wang, and L. Zhang (2005), Frequency analysis of nonidentically distributed hydrologic flood data, *J. Hydrol.*, *307*, 175–195.

Sivapalan, M., G. Blöschl, R. Merz, and D. Gutknecht (2005), Linking flood frequency to long-term water balance: Incorporating effects of seasonality, *Water Resour. Res.*, *41*, W06012, doi:10.1029/2004WR003439.

Strahler, A. (1952), Hypsometric (area-altitude) analysis of erosional topography, *Bull. Geol. Soc. Am.*, *63*, 1117–1142.

Waylen, P., and M. Woo (1982), Prediction of annual floods generated by mixed processes, *Water Resour. Res.*, *18*(4), 1283–1286.

Wood, E., and C. Hebson (1986), On hydrologic similarity: 1. Derivation of the dimensionless flood frequency curve, *Water Resour. Res.*, *22*(11), 1549–1554.

Woods, R. (2003), The relative roles of climate, soil, vegetation and topography in determining seasonal and long-term catchment dynamics, *Adv. Water Resour.*, *26*(3), 295–309.

————————————

P. Allamano, P. Claps, and F. Laio, Dipartimento di Idraulica, Trasporti ed Infrastrutture Civili, Politecnico di Torino, Corso Duca degli Abruzzi, 24, I-10129 Torino, Italy. (paola.allamano@polito.it)